Spring 2018

Galvanic and Pitting Corrosion of a Fastener Assembly

Julie Shallman
jms450@zips.uakron.edu

GALVANIC AND PITTING CORROSION OF A FASTENER ASSEMBLY

A Honor's Project

Presented to

The Honor's College of The University of Akron

In Partial Fulfillment

of the Requirements for the Degree

Bachelor of Science

Julie Marie Shallman

May, 2018

ABSTRACT

This research focuses on coupled galvanic/pitting corrosion of AA7075 when combined with stainless steel in a fastener assembly. A one-dimensional mathematical model of a well-mixed thin film electrolyte is developed to predict the damage profile of the AA7075 surface when its protective coating is damaged. The damage exposes the galvanic couple. A time dependent system of partial differential equations for potential, chloride concentration, aluminum ion concentration, and damage is developed and solved numerically. Two approaches to calculate the current density within aluminum pits are discussed. The first is a current balance between the cathodic, anodic and passive portions of the metal surfaces. This reflects the local chemistry that drives pit growth early on before any growth of oxide to repassivate the metal. The second approach is based on the work of McKinnon [1], using the potential calculated at the bottom of each initiated pit with a polarization curve relevant to the pit chemistry. This approach reflects the growth of pits during the formation of oxide, and leads to the repassivation of pits. Now that the model and solution scheme have been formulated, the next step is to carry out the simulation, and compare results to experimental results.

TABLE OF CONTENTS

LIST OF TABLES

LIST OF FIGURES

CHAPTER I

INTRODUCTION

The focus of this research is to develop a one-dimensional mathematical model to predict the damage profile of galvanically induced pitting corrosion on an AA7075 surface when coupled with stainless steel in a fastener assembly. We examine the scenario where an AA7075 surface with steel bolts in it, has its protective coating damaged and the steel and aluminum surfaces are exposed. A well-mixed thin electrolyte film is present and in contact with the metal surfaces. We develop a system of partial differential equations (PDE's) to determine the bulk potential, chloride concentration, aluminum ion concentration, initiation of pits, the current density in the pits, and how the aluminum surface corrodes in space and time. The model is based on the idea that the galvanic couple keeps the bulk potential sufficiently high enough to allow initiation of pits. The local current density must be accurately determined to predict realistic damage from local corrosion. The use of pencil electrodes helps to determine local current density and defines the model as a series of uncoupled pencil electrodes. Eventually, localized corrosion transitions to activated corrosion as pits coalesce based on the approach from McKinnon's work in [1]. Then the anodic current density reverts back to the current density related to the bulk polarization curve per the work done by Clark, Lillard, and Haque [4].

It is important to note there is a small crevice between the two metal types in the fastener assembly. The work done by Roland [2] considers the corrosion on the aluminum surface in the crevice between the steel and aluminum. Unlike [2], this research focuses on the aluminum surface outside of the crevice. Thus our work, in addition to Roland [2], will allow one to examine the corrosion on the entire aluminum surface.

This research is relevant because many industries utilize differing metal types to reduce weight and cost of products. For example, in aerospace designs, light weight aluminum alloys are paired with denser bolts to make the body and wings light but able to support significant load. This research provides a predictive model of damage on the aluminum surface. This provides a tool to help determine the lifetime of the fastener assembly's structure.

1.1 Galvanic Corrosion

Galvanic corrosion is an electrochemical process that affects unstable metals coupled together. It is much more aggressive than the corrosion of a single metal type. There are three criteria that must be met for galvanic corrosion to occur: two or more dissimilar metals are present, they are in electrical contact, and they are exposed to an electrolyte. These elements create a corrosion cell, with one metal acting as the cathode, the other as the anode, and the electrolyte allows ion migration. Each metal type has a tendency to become active in the presence of an electrolyte, when measured, this tendency is called its electrode potential. These electrode potentials

are higher for the more noble metals; metals that are more stable in their natural state. Thus whichever metal has the higher electrode potential acts as the cathode of the cell, and the other is the anode of the cell. The cathode experiences a reduction reaction, and gains electrons. While the anode experiences an oxidation reaction, and loses electrons, allowing the dissolution of metal into ions. Thus, the damage occurs on the surface of the anodic metal.

1.2 Localized Corrosion

In the corrosive galvanic environment created by the dissimilar metals under investigation in this honor's project, localized corrosion is observed on the anodic aluminum surface. Localized corrosion is the corrosion of a small specific area when the metal surface is in contact with a corrosive environment. There is accelerated dissolution and breakdown of the passive film in these specific areas of the metal. These small areas have extreme local chemistries, compared to the surrounding areas, and are under a higher rate of chemical attack. There are different types of localized corrosion; pitting, stress cracking, chloride stress, caustic stress, and others. We specifically focus on pitting.

Localized pitting corrosion is an important, relevant, and complex issue. The complexity comes from multiple factors, the first being the small scale where this corrosion happens. The passive film and depth of the pits is only nanometers in magnitude. Secondly, the rate at which the dissolution of metal occurs starts out extremely high and then slows. This causes rapidly moving boundaries. Thirdly,

the chemistry that drives the rate of metal damage constantly changes as well, thus tracking the chemistry is complex. Fourthly, it is extremely difficult, if not impossible, to predict exactly where and when localized corrosion will occur. Lastly, the beginning stage of pitting is the least understood part of the entire problem.

1.3 Literature Review

There are numerous works that investigate galvanic corrosion of metals. For our purposes we cite those most relevant to our model development. Stenta [5] assumes a well-mixed electrolyte, uniform species concentration, proper no flux conditions at the electrolyte boundaries, and proper surface behaviors between the metals and the electrolyte to examine galvanic corrosion. In all of these cases the governing equation of potential in the electrolyte is the Laplace Equation. Stenta includes a proposition for a 1D model to track the damage evolution of the anodic surface. Both cartesian and cylindrical geometries are investigated. Numerical solutions are compared to GalvanicMaster (now CorrosionMaster), a software package which uses the bulk potential profile to calculate the damage profile of a metal surface through time. Unlike Stenta's work, this paper only uses the bulk potential for determining the initiation of pits. The determination of the damage profile for an aluminum surface due to pitting corrosion is based on the potential and associated current density in the pits.

Later work done by Stenta [6] focuses on a species driven model to determine the damage done to nickel. This work shows that the work done with the assump-

tion of a well-mixed electrolyte still holds true for thicker electrolyte depths. The conclusion of this paper is very important for this paper when dealing with local concentrations and using the well-mixed electrolyte assumption.

Laycock and Newman [7] investigate stainless steel and the effects of galvanic corrosion. They conclude there are two types of pit growth: mixed activation/ohmic growth when the potential is lower, and diffusion controlled growth with a metal salt film present when the potential is higher. In addition, [7] concludes that pitting potential is a function of chloride concentration. The work done by Galvele [8] agrees, and a potential as a function of chloride is defined. Laycock and Newman's model predicts real pits will also grow in either the active or salt-filmed states depending on current density. Thus as proposed here, current density is a function of potential, which is dependent on the local chloride concentration.

Steel has largely been researched for metastable pitting. Frankel, Stockert, Hunkeler, and Boehni [9] discuss the initiation, growth, decay, and pit stability criteria of pitting in steel. The pits observed are hemispherical in shape, and the current density present is a function of time. Specifically, current density is found to be constant over the pit area in the early stage of growth, and depends on the local potential and chloride concentration. These findings are used in principle for the aluminum in this model, but the pit shape is assumed to be cylindrical in shape.

More recently, Frankel, Matzdorf, Nickerson, Troconis, Li, Buchheit, and Feng have studied aluminum and its alloys in [10, 11]. Specifically, AA7075 coated panels with scribed and unscribed through-holes and Ti and steel fasteners. The

system is tested in a salt-fog chamber to study beach-like atmospheric corrosion. Frankel and Feng [11] find that accelerated galvanic corrosion was experienced in scribed AA7075 panels when paired with steel fasteners. The steel bolts caused more damage than the Ti bolts, even though Ti is a more noble metal, due to the higher cathodic current generated by the steel. It is found that the anodic current of the panel depends on the number of bolts present, and that the total cathodic current of the fasteners is equal to the anodic current.

The current density is an important value in the localized pitting process, and is discussed throughout the literature. Galvele [8] specifically developed a pit model based on the assumptions that metal ions hydrolyze in pits and corrosion products leave the pit by diffusion. His work concludes the presence of high potential allows proper current density and proper pH values for localized corrosion to occur. In steel it is seen that with high enough potentials pits form and the current density present in the pits is independent of the bulk, and much higher. Galvele shows current density is linked to critical pH values and the repassivation of pits. He concludes that the presence of acid salts increases pitting potential and that the higher current density in pits must be accounted for.

In Galvele's model [8] he makes some important modifications to previous work: i) simplifications to the transport equations of the pit yields that only transport by diffusion is present ii) the expression for the anodic reaction in the pit is generalized, and the dissolution of metal only occurs at the bottom of the pit, allowing unidirectional pit growth, iii) the hydrolysis equilibrium reaction is reached

quickly and thus simplifies the description of the pitting processes, iv) the anion salt is assumed to act as a supporting electrolyte for the ionic species formed from dissolution in the pit. These assumptions agree with the work done here.

Similar to this work, Roland [2] studies a steel and Al7075 fastener assembly and the galvanic, pitting, and crevice corrosion occurring. The formulation and solution to differential equations determines the potential in the bulk electrolyte, and the potential, oxygen concentration, and aluminum ion concentration profiles in the crevice. The aluminum ion concentration builds up at the mouth of the crevice, and the area with the greatest aluminum ion concentration experiences the greatest damage due to a higher level of chloride ions and subsequent increased pit initiation. He investigates the current balance in the crevice and its consequences on the bulk potential profile.

In combination with this current work and the work of Roland [2], Dr. Golovaty solves the Laplace Equation for potential over the entire domain of the system [12]. Through personal communication we have the summary of his findings, and use it in addition to Roland's work to develop the current balance of the system.

The work done by Colwell [3] tracks the accumulation and formation of metastable pits and stable pit densities, through a mathematical stochastic pit initiation model. The model uses the kinetic Monte Carlo method and Galvele criterion, the product of current density and pit depth exceeding a critical value, to simulate localized corrosion of an aluminum surface. Colwell determines the formation of metastable pits and their transition to stable growth through time. The model

creates a 3D surface of chloride concentration, potential, and likelihood to pit. These results are in agreement with the experimental data for AA7075, from the work of Cavanaugh, Birbilis, and Buchheit [13], and AA1050, from the work of Elola, Otero, and Porro [14]. This 3D surface is utilized in this honor's project.

Brackman [15] investigates the crevice corrosion damage evolution of a nickel surface. He uses an asymptotic analysis to simplify the governing equations, and develops a mathematical model to predict the damage evolution through time. The model also provides new insights into crevice corrosion. Brackman utilizes the Divergence Theorem over two subdomains, the bulk, and the crevice. In this thesis we also split the Divergence Theorem to analyze the current balance of the system.

McKinnon [1] develops a 1D pencil electrode model with stages of pitting to predict the damage profile of a metal surface due to pitting corrosion. The three stages of growth are based on certain potential values being reached. The first stage is ohmic controlled, the second is diffusion controlled, and the third is again ohmic controlled. A downward scan of the working electrode potential is performed to reach the transition potential value to switch the pit to its third stage. This artificially holds the potential high enough to stay in the diffusion growth stage, and allows the pit to grow long enough to match known experimental data of damage. The ohmic controlled growth is governed by Faraday's law, as in this work. The main contribution of McKinnon's work to this honor's project is the calculation of the potential drop in a pit.

Mizuno and Kelly [16, 17] are a series of two papers investigating the effects

of atmospheric exposure on aluminum alloy AA5083 and steel couples. The first paper in the series, [16], characterizes experimental data for electrochemical kinetics of steel in salt solutions. The influence of these conditions on the degree of sensitivity, intergranular corrosion propogation, and potential are studied as well. In the second paper, [17], a mathematical model is developed to predict the intergranular corrosion damage of the aluminum surface. The Laplace Equation is used to calculate the potential distribution in the system based on experimental boundary conditions. The model predicts damage depth after 100 hours in different sodium chloride solutions. Throwing distance is described here as the minimum distance from the steel fastener where no damage occurs. Results show that calculated throwing distance and maximum pit depth are overestimated compared to experimental data. This overestimation is from the adjusted polarization curve based on experimental results found in [16]. Thus Kelly acknowledges that an adjusted current density is needed to have the correct magnitude of throwing distance and damage depth. The adjusted current density is orders of magnitude larger than the unadjusted current density from the unadjusted polarization curve. Thus in this paper we have current density in the pits based on local chemistry and not the bulk potential.

The adjusted current density discussed by Mizuno and Kelly [17], is investigated further by Haque, Clark, and Lillard [4]. In [4], the commercial software package model predictions of damage depth profiles are compared to experimental data of an aluminum/copper system. It is found that the model predictions underestimate the damage done to the anodic surface by pitting corrosion. The software

package correlates current density to a potential mesh point through experimental potentiodynamic polarization curves. Haque, Clark, and Lillard [4] specifically discuss how this methodology presents a problem for pitting corrosion, i.e. AA7075 in a chloride solution. In the case of pitting corrosion, the average surface current density determined by polarization curves is not equal to the current density at the bottom of a pit. The surface current density is found to be orders of magnitude smaller than the current density in the pit, resulting in the underestimated damage profiles of previous models. In addition, Haque presents a method to determine a polarization curve that provides a more accurate current density for pitting corrosion when used as input data for commercial software packages. Unlike [4], in this paper we investigate AA7075 and steel, our electrolyte depth is much shallower, and a crevice is present between the metals. But, we do use the the theory of relevant current density at the bottom of a pit being much larger than the current density calculated from the bulk potential profile of a couple.

1.4 Description of the Model

Galvanic and pitting corrosion occur on the aluminum surface because of the galvanic interaction between the steel and AA7075. The potential in the bulk electrolyte, and the chloride concentration are the environmental features that determine whether the aluminum surface will pit or not. From the likelihood to pit surface from Colwell [3], we determine whether a pit is likely or not to form at a specific area on the aluminum surface. The likelihood to pit depends on the bulk potential, and the local chloride

concentration; note that the higher these values are, the more likely a pit is to form. This bulk potential is used as the potential at the top of the pit, E, and the potential at the bottom of the pit, E_{bot}, follows from the calculated potential drop in the pit, ΔE. The value ΔE is the change in potential from the top of a pit to its bottom, and is calculated from equations (28) and (29) from McKinnon [1]:

$$\xi = \frac{-\gamma A_{sat} + \sqrt[2]{\gamma^2 A_{sat}^2 + N a_{blk} C}}{N a_{blk}},$$

$$\Delta E = E - E_{bot} = -\frac{1}{\alpha} ln(\xi).$$

Here A_{sat} is the concentration of aluminum ions the electrolyte can hold in solution. The value of sodium ions present in the electrolyte is Na_{blk}, C is the concentration of chloride, the value of γ is a ratio of the electrolyte saturation limit of aluminum ions, and α is the constant representing F/RT. Both equations depend on the local concentration of chloride in the bulk electrolyte. The speed at which the pit grows is determined by the current density at the bottom of the pit. As the pit grows deeper, aluminum ions migrate to the bulk and initially raise the local chloride concentration at the top of the pit, due to electroneutrality. Subsequently, aluminum chloride forms and the local concentration of chloride decreases. The damage done to the pit increases the thickness of the electrolyte, which subsequently reduces the potential drop, and thus increases the bulk potential profile, allowing other spots on the surface to initiate pits. Hence the cycle continues, more pits form and additional damage occurs in each pit. We discuss repassivation through two different theories. The first approach to repassivation follows the work done by McKinnon [1]. The second

approach to repassivation follows the theory postulated in [4].

Experiments conducted by Dr. R. S. Lillard's team have supplied us with a bulk polarization curve for the metal couple, a pit polarization curve of pure aluminum, and the conductivity value in the electrolyte film. The bulk potential is calculated using the bulk curve and the conductivity. The pit curve shows the general behavior of the current density in a pit given an E_{bot} value. Once the current density is known, the damage depth of the pit is calculated using Faraday's Law.

We do not have a pit polarization curve enabling us to determine the current density at every spatial location of a pit surface over time. Hence, in the mathematical model each pit is looked at as its own individual 1D pit. This means the sides of each pit are inert and only the bottom of the pit is corroding. This is because it is assumed there is no diffusion in the pit parallel to the active bottom surface. The pits are evaluated at each point along the aluminum surface individually and do not affect neighboring pits. Each pit has its own time of initiation and damage. The completed algorithm's outputs of damage over time are compared for accuracy against experimental data provided by the Lillard team.

CHAPTER II

MODEL FORMULATION

This model is based on the physical situation shown in Fig (2.1) when an AA7075 surface is paired with a more noble metal, stainless steel, fastener. The couple potential induces a much higher potential than the open circuit potential of AA7075, thus there are higher potentials in the bulk electrolyte. With sufficient levels of local chloride concentration pitting corrosion initiates on the AA7075 surface. We postulate that as damage increases on the aluminum surface the bulk potential profile increases. It is known that as damage increases the local chloride concentration increases by electroneutrality effects to balance the charge of the released aluminum ions from corrosion. The combination of increased bulk potential and local chloride concentration causes new pits to initiate further along the AA7075 surface.

Within the pits the anodic current density is significantly higher than the current density found from the bulk polarization curve. This is due to localized corrosion effects in the pits. The anodic current density is found to be directly related to the available cathodic current in the experiments done in [10, 11]. One can mathematically demonstrate the experimental result of pit current density being directly related to total cathodic current, using the Divergence Theorem, a current balance procedure, and proper assumptions. The simplifying assumptions are: i) each

pit is isolated from all neighboring pits; ii) pit shapes are rectangular in 2D systems and cylindrical in 3D systems; iii) the walls of the pits are inert surfaces; iv) only the bottom surface of pits, a line in a 2D system or a circle in a 3D system, are active. Another approach, described by Haque, Clark, and Lillard in [4], is to use a measured pit polarization curve and bulk potential values to determine pit current density. The bulk potential values are used because the electrolyte domain is described using a thin domain approximation.

By Faraday's Law and under anodic current density, the pits continue to grow as described by the current balance approach above. However, the experiments in [4] indicate that at some point the magnitude of the anodic current drastically decreases in magnitude. It is unclear why this occurs, but there are two possible answers: i) similar to the work done by McKinnon [1], or ii) similar to the work done by Lillard, Clark, and Haque in [4]. In the first approach the potential drop in the pits is calculated based on the equations provided in [1]. Using the bulk potential and the calculated potential drop the relevant potential at the bottom of the pit is known, and used to determine the anodic current density in the pit. As the potential drop increases the anodic current density at the bottom of the pit decreases and the pits repassivate. In the second approach the pits coalesce and the damaged surface begins to act as a single active surface with anodic current density related to the bulk potential profile. Regardless of which approach is used it is unknown when the drop in anodic current density occurs. Based on Figure 10 of [4], this model assumes it occurs around an anodic current density of $0.005\frac{Amp}{cm^2}$.

The governing equations necessary to accomplish the proposed model are developed in the following subsections.

2.1 Bulk Governing Equations

Conservation of mass is described by the Nernst-Planck equation, a representation of the flux of an ionic species in a fluid medium. In general, the transport of ions is expressed as

$$\frac{\delta C_i}{\delta t} = -\nabla \bar{J}_i, \tag{2.1}$$

where i represents the ionic species, C_i is the concentration of the species and $\bar{J}_i$ is the flux of the species. The species' flux is expressed as

$$\bar{J}_i = -D_i \nabla C_i - n\frac{FD_i}{RT} C_i \nabla E + \bar{u} C_i. \tag{2.2}$$

This equation describes, respectively, the movement of ions in the bulk electrolyte based on the gradient of species concentration (diffusion), the gradient of potential (electromigration), and convective transport due to fluid velocity (convection). In equation (2.2) D_i is the diffusivity, C_i is the ionic concentration, n is the valence of the ionic species, F is Faraday's constant, R is the gas constant, T is the temperature, E is the potential in the electrolyte, and $\bar{u}$ is the velocity of the fluid. In our problem the electrolyte is not moving, thus

$$\bar{u} = \bar{0}. \tag{2.3}$$

We also assume the bulk electrolyte is well-mixed, meaning the ionic species have no concentration gradients in space. Thus,

$$\nabla C_i = 0. \tag{2.4}$$

By equations (2.3) and (2.4), we see that (2.2) simplifies to

$$\bar{J}_i = -n\frac{FD_i}{RT}C_i\nabla E. \tag{2.5}$$

It easily follows that equation (2.1) simplifies as well, to

$$\frac{\delta C_i}{\delta t} = -\nabla\left(-n\frac{FD_i}{RT}C_i\nabla E\right). \tag{2.6}$$

The system is stable and therefore follows the condition of electroneutrality. This condition implies that the total system charge from the cations and anions in the system must balance each other. Therefore, the overall charge of the electrolyte must be neutral, or zero, $\sum_i n_i C_i = 0$. Thus equation (2.6) results in

$$\sum n_i\frac{\delta C_i}{\delta t} = \nabla\sum_i\left[n_i^2\frac{D_iF}{RT}C_i\nabla E\right] = 0. \tag{2.7}$$

Further simplification yields

$$\sum_i n_i^2\frac{D_iF}{RT}\nabla C_i\nabla E + \sum_i n_i^2\frac{D_iF}{RT}C_i\nabla\left(\nabla E\right) = 0. \tag{2.8}$$

From our assumption that the electrolyte is well-mixed the first term in the above equation is eliminated and we are left with the following expression:

$$\sum_i n_i^2\frac{D_iF}{RT}C_i\nabla\left(\nabla E\right) = 0. \tag{2.9}$$

It is known that $\sum_i n_i^2\frac{D_iF}{RT}C_i > 0$, hence the governing equation simplifies to the Laplace Equation $\nabla^2 E = 0$.

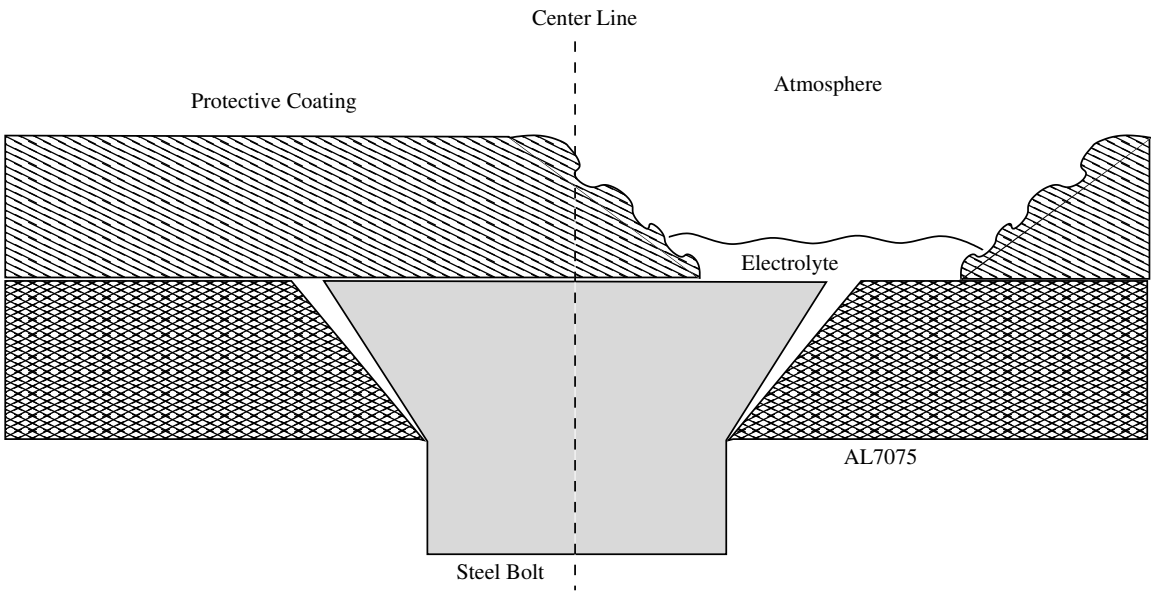

Figure 2.1: The aluminum surface with a steel bolt and absent section of protective coating.

2.1.1 Boundary Conditions of Bulk

The actual geometry of our galvanic system is shown in Fig (2.1). The geometry is complex. In Fig (2.2), a simplified geometry is shown; this idealized domain is used for the development of our mathematical system. The left and right boundaries are the metal coating, which are assumed to be impermeable. The top boundary is where the atmosphere and the electrolyte meet, and we assume no ions are lost to the atmosphere. Thus the top, left, and right boundaries have a no-flux condition. The no-flux condition is mathematically expressed as

$$\bar{J}_i \cdot \hat{n} = 0. \tag{2.10}$$

Here $\hat{n}$ is the unit outward pointing normal vector to the boundary of the system. Given equations (2.5) and (2.10), we find the no-flux condition simplifies to

$$\nabla E \cdot \hat{n} = 0. \tag{2.11}$$

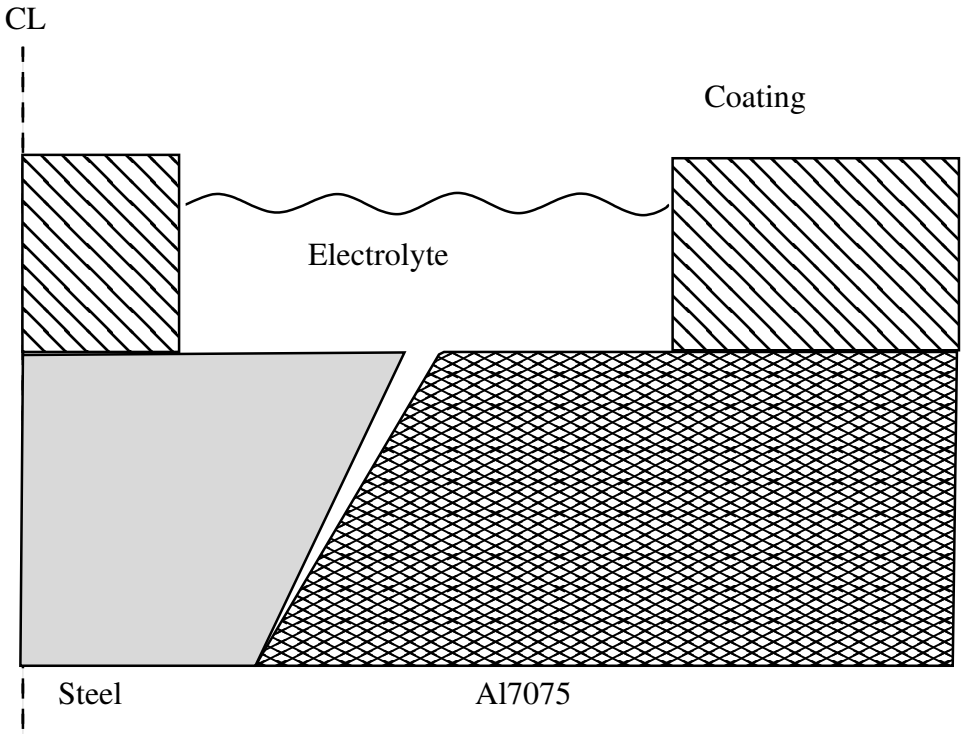

Figure 2.2: The idealized domain.

Since both the steel and aluminum surfaces are reacting with the electrolyte, the bottom boundary condition of our domain is Ohm's Law,

$$-\kappa \nabla E \cdot \hat{n} = i(E). \tag{2.12}$$

The constant κ is the electrolyte conductivity, and $i(E)$ is the current density as a function of potential.

In our two-dimensional setting we represent the Laplace Equation as

$$\nabla^2 E = E_{xx} + E_{zz} = 0. \tag{2.13}$$

Here the vertical axis is z, and the horizontal axis is x.

We have the no-flux condition on the left and right boundaries as seen in Fig (2.3) thus,

$$E_x = 0, \quad \text{at} \quad x = -L_1 \tag{2.14}$$

$$E_x = 0, \quad \text{at} \quad x = L_2. \tag{2.15}$$

The total depth of the film to the bottom of the damage in the aluminum is expressed as $z = w(x) + h(x,t)$. Here, the depth of the film from the undamaged metal surface to the top of the film is $w(x)$, and the damage into the aluminum surface is $h(x,t)$. We define a level curve for the gas/liquid surface of the electrolyte film as $F = z - w(x) = 0$. Note that the gradient of F, $\nabla F = \langle -w_x, 1\rangle$, is perpendicular to the level curve of F. The normal vector of F is

$$\hat{n} = \frac{\nabla F}{|F|} = \frac{\langle -w_x, 1\rangle}{\sqrt{w_x^2 + 1}}. \tag{2.16}$$

The gradient of potential dotted with the normal vector of the level curve F is zero by equation (2.11), at surface $z = w(x)$,

$$\langle E_x, E_z\rangle \cdot \frac{\langle -w_x, 1\rangle}{\sqrt{w_x^2 + 1}} = 0. \tag{2.17}$$

We assume a thin domain in the electrolyte, therefore the depth w is much smaller than the total length of the exposed metal surfaces, $L = L_1 + L_2$. When

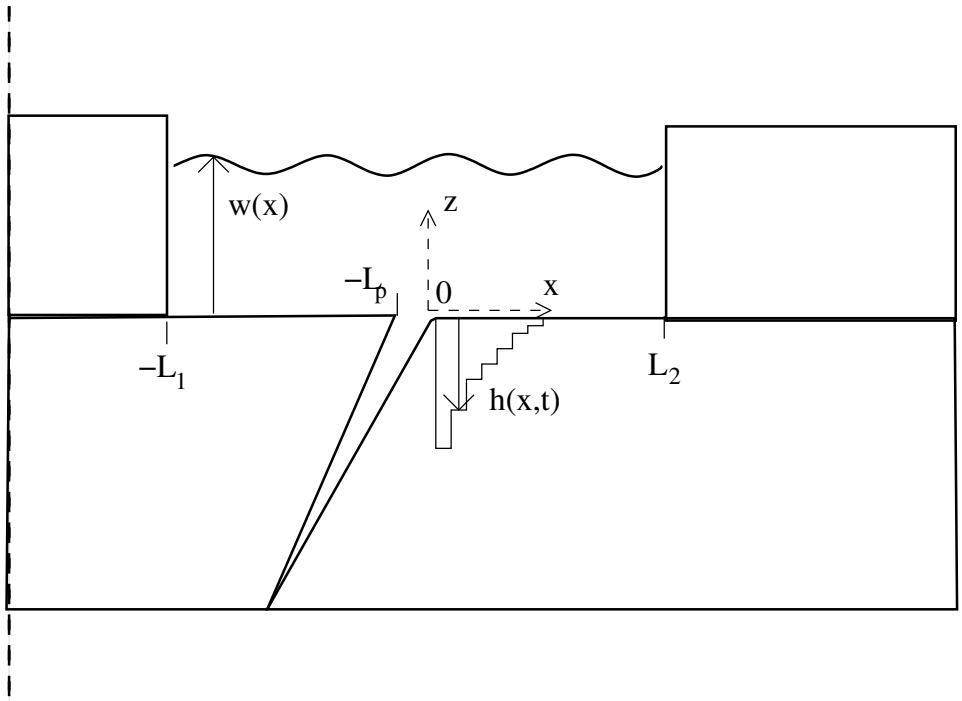

Figure 2.3: The measurements of idealized domain.

analyzing w_x we assume $\frac{dz}{dx}$, which is approximately $\frac{w}{L}$, to be a very small number. Thus w_x is small and w_x^2 is even smaller. This thin domain assumption allows us to approximate

$$\sqrt[2]{w_x^2 + 1} \approx 1. \tag{2.18}$$

Hence equation (2.17) simplifies to the boundary condition at $z = w(x)$,

$$E_x w_x = E_z. \tag{2.19}$$

Next we consider the bottom boundary of our system. Here $z = -h(x,t)$, and we define $F = -h - z$. It follows that

$$\nabla F = \langle -h_x, -1 \rangle \tag{2.20}$$

Thus the normal to the surface F is,

$$\hat{n} = \frac{\langle -h_x, -1 \rangle}{\sqrt{h_x^2 + 1}}. \tag{2.21}$$

Similar to the top boundary condition, we analyze h_x assuming $\frac{dh}{dx}$ is approximately $\frac{w}{L}$. Thus h_x is a small number, and h_x^2 is an even smaller number, and $\sqrt{h_x^2 + 1} \approx 1$. Hence, the norm of F simplifies to

$$\hat{n} = \langle -h_x, -1 \rangle . \tag{2.22}$$

By equations (2.12) and (2.22), Ohm's Law at the bottom boundary of the system is

$$-\kappa(-E_x h_x - E_z) = i(E). \tag{2.23}$$

Note that over the passive aluminum surface and the steel surface there is no damage, thus $h(x,t) = 0$. Hence, the general bottom boundary condition is

$$\frac{i(E)}{\kappa} - E_x h_x = E_z. \tag{2.24}$$

We also assume that the walls of each pit are inert. Thus the bottom of the pit is the only active surface and causes damage only in the vertical direction down into the aluminum. There is no dissolution of aluminum in the horizontal direction, allowing the pits to be individual entities. The active and nonactive surfaces of each pit are depicted in Fig (2.4).

Now that we have all of the necessary boundary conditions, we look again at the governing equation, equation (2.13). At this point Stenta [5] performs an asymptotic procedure for the thin domain assumption, allowing $E(x,z,t) = E(x,t)$.

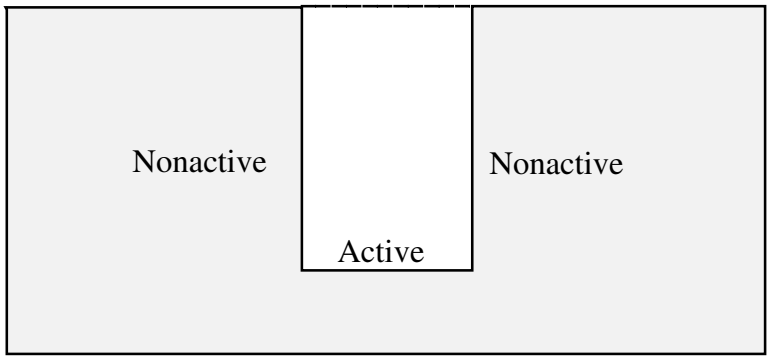

Figure 2.4: Each individual pit represented has inert walls and active pit bottom.

Instead of using this asymptotic procedure, we integrate the two-dimensional Laplace Equation with respect to the vertical axis. We assume the potential will change with respect to the length of the metal surface, x, and not vary much with respect to the electrolyte depth, z, over each point of the metal surface. Hence,

$$\int_{-h}^{w} E_{xx} + E_{zz} dz = 0, \tag{2.25}$$

$$E_{xx}(w+h) + E_z|_{z=w} - E_z|_{z=-h} = 0. \tag{2.26}$$

Our top and bottom boundary conditions, equations (2.19) and (2.24), simplify equation (2.26) to

$$E_{xx}(w+h) + E_x w_x + E_x h_x - \frac{i(E)\sqrt{h_x^2+1}}{\kappa} = 0 \tag{2.27}$$

$$E_{xx}(w+h) + E_x(w+h)_x - \frac{i(E)\sqrt{h_x^2+1}}{\kappa} = 0 \tag{2.28}$$

$$\kappa \left[E_x(w+h)\right]_x = i(E)\sqrt{h_x^2+1}. \tag{2.29}$$

Our 1D equations from integration are consistent with the work done by Stenta [5],

where he used thin domain asymptotics to justify the 2D problem being represented by a one dimensional system.

Next we assume since h_x is small, so h_x^2 is much smaller, and thus $\sqrt{h_x^2+1}$ approaches 1, and so equation (2.29) becomes

$$\kappa \left[E_x(w+h)\right]_x = i(E). \tag{2.30}$$

It is important to note that the above equation can be expressed specifically for both the surface of the steel and of the aluminum, where $h(x,t) = 0$ for the steel. This is because steel is the cathode and is not experiencing galvanic corrosion. In addition, our surface has three portions; steel, the crevice, and aluminum. Each section contributes to the total current density profile, but over the crevice we assume $i = i_{fixed}$. This is because the work done by Roland shows that the current density at the mouth of the crevice is nonzero and contributes to the current balance of the entire system, this concept is further discussed later in Section 2.5. Thus the current density over the surfaces, $i(E)$, can be expressed as being composed of the contributing components, $i_c(E)$, i_{fixed}, and $i_a(E)$. Here $-i_c(E)$ is the current density over the steel and $i_a(E)$ is the current density over the aluminum. Since Ohm's Law only applies to the steel and aluminum surfaces, we have

$$\kappa \left[E_x w\right]_x = -i_c(E) \tag{2.31}$$

for the cathodic steel, and

$$\kappa \left[E_x(w+h)\right]_x = i_a(E) \tag{2.32}$$

for the anodic aluminum.

Equation (2.30) is the ordinary differential equation used by Stenta [5], and in the present work. From any of the above equations E_{xx} can be solved for and seen to be a function of the current density i. The second derivative of a function is the convexity of the function. This helps the understanding of the shape of the bulk potential profile we develop from the experimental data provided by the Lillard team. We see that over the steel surface $i < 0$ thus potential is concave down, and when $i > 0$ over the aluminum surface, the potential is concave up.

2.2 Species Governing Equations

Now we focus on the governing equations of the concentration of ions in the system. It is important to note that we use local concentrations as a driving force in our proposed model. This implies that our electrolyte is in fact not well-mixed. From the work by Stenta [6] it is shown that well-mixed assumptions can still be used in systems with thicker bulk electrolytes. Later it will be shown that bulk electrolyte depth is magnitudes larger than the damage depth, and thus is considered thicker. This allows us to still simplify the Nernst-Planck equation to the Laplace Equation for potential. As will be shown, the electrolyte potential is nearly a constant throughout the bulk. Hence, we solve for the species distribution under this assumption.

In a system with three unknowns, A, C, and E, there are three equations to solve the system: the PDE for aluminum ions, the PDE for chloride, and electroneutrality of species. These equations are developed later in this section. With E

being assumed constant, $E_x = 0$, and thus the PDE's for species concentrations have electromigration terms equal to zero. The system of equations is then over specified and there are only two independent equations: the PDE of aluminum ions and the PDE of chloride without potential being accounted for. Thus A and C are solved using the equations developed in this section, and the solution for E using the ODE, equation (2.30), is developed further in Chapter 3.

To solve for the concentration of chloride in the electrolyte we use the principle of electroneutrality

$$C = 3A + Na_{blk}. \tag{2.33}$$

Here C is the concentration of chloride, A is the concentration of aluminum ions, and Na_{blk} is the constant concentration of sodium ions in the bulk electrolyte. This expression for chloride is based on local species chemistry as the driving force for ion concentrations.

The calculation of aluminum ion concentration is based on the basic principle of transport phenomena, the conservation of mass of each species. The concentration of a species is calculated with the general partial differential equation,

$$\begin{aligned} C_{it} = DC_{ixx} + \frac{\hat{K}}{(w+h)}(C_{iout} - C_i) \\ + \frac{iM}{Fn(w+h)} + \frac{nFD}{RT}(C_i E_x)_x + (S^+ - S^-). \end{aligned} \tag{2.34}$$

$$\tag{2.35}$$

Here DC_{ixx} is the diffusion of species C_i ions through space, $\frac{\hat{K}}{(w+h)}(C_{iout} - C_i)$ is the mass transfer of the species in and out of the system through the electrolyte/air inter-

face and $\hat{K}$ is the mass transfer coefficient, $\frac{iMw}{Fn(w+h)}$ is the oxidation surface reaction that occurs at the metal/electrolyte interface, $\frac{nFD}{RT}(C_iE_x)_x$ is the electromigration of the ion, and $(S^+ - S^-)$ is a general bulk reaction term for source and sink reactions of the species. The mass transfer and surface reaction terms come from integrating the two dimensional equation for the concentration of a species C_i with respect to z. The boundary condition of $C_{iz}|_{z=w}$ is the interface of air with the electrolyte. Here ions can enter the electrolyte or leave the electrolyte. Thus, the species can transfer in and out of the system. For the boundary condition of $C_{iz}|_{z=-h}$ we consider the metal surface reaction. Here the metal ions leave the surface due to dissolution.

For the PDE of aluminum we assume there is only diffusion of ions through the electrolyte, a surface reaction term due to the dissolution of the aluminum metal surface at the bottom of the pits, and a sink term from the chloride and aluminum ion reaction in the bulk. The mass transfer term is assumed to equal zero, since the air does not contain aluminum ions to enter the system and the aluminum ions are not leaving the electrolyte through the air. The electromigration term is set equal to zero by the assumption of small potential gradients in the bulk. It is important to note that Roland [2] does not include a bulk reaction sink term to the equation for aluminum ion concentration. This is because the formation of aluminum chloride does not occur until the concentration of aluminum ions exceeds $0.003\frac{mol}{cm^3}$, as seen in Fig (2.5) from Roland [2]. In Roland's work the concentration of aluminum ions is always below the critical value, and in this honor's project the bulk reaction sink term is included because the critical concentration of aluminum ions may eventually

be surpassed. To account for both the formation, and absence, of aluminum chloride we have a piecewise expression for aluminum ion concentration. Thus A with respect to time is

$$A_t = \begin{cases} DA_{xx} + \frac{i_{pit}M}{3F(w+h)} & \text{if} \quad A < 0.003\frac{mol}{cm^3} \\ DA_{xx} + \frac{i_{pit}M}{3F(w+h)} - KC^3A & \text{if} \quad A \geq 0.003\frac{mol}{cm^3}. \end{cases} \tag{2.36}$$

Here A is the concentration of aluminum ions, K is the reaction rate constant for the formation of aluminum chloride, the surface reaction is a function of i_{pit}, the current density in the pit, and C is the concentration of chloride in the system.

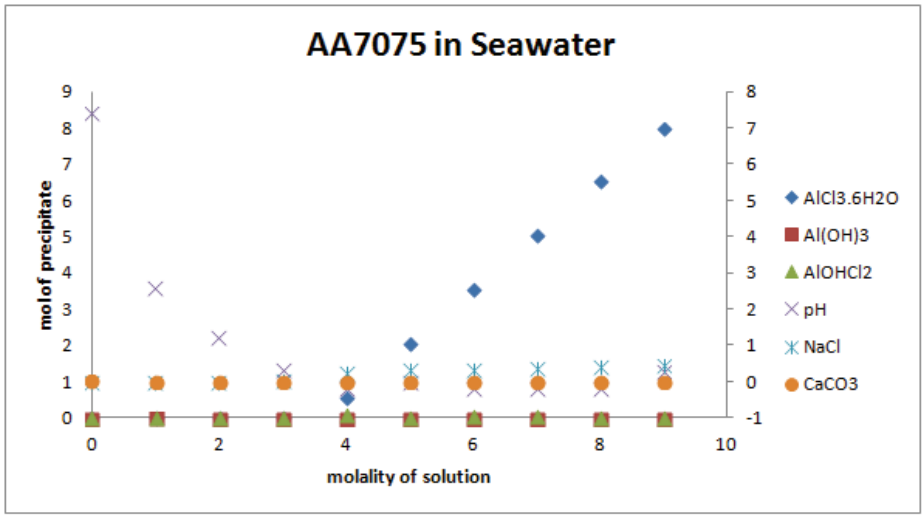

Figure 2.5: The necessary concentration of aluminum for the formation of the aluminum chloride. Taken from Roland [2].

The value of aluminum ion concentration in the crevice is also investigated when the anodic current density in the crevice is varied, as seen in Fig (2.6) from Roland [2]. It is shown that the larger the anodic current density is the larger the concentration of aluminum ions. This shows that the much larger current density values

seen in this honor's project may lead to high enough aluminum ion concentrations for the bulk reaction sink term to be significant. As the aluminum ion concentration increases, the concentration of local chloride increases due to electroneutrality and surpasses the critical concentration value found from Colwell's surface boundary, and thus a pit initiates. In addition, as the aluminum ions diffuse horizontally along the aluminum surface in the bulk electrolyte, the aluminum ion concentration increases further from the crevice and pits continue to initiate further along the aluminum surface due to local increases in chloride concentration.

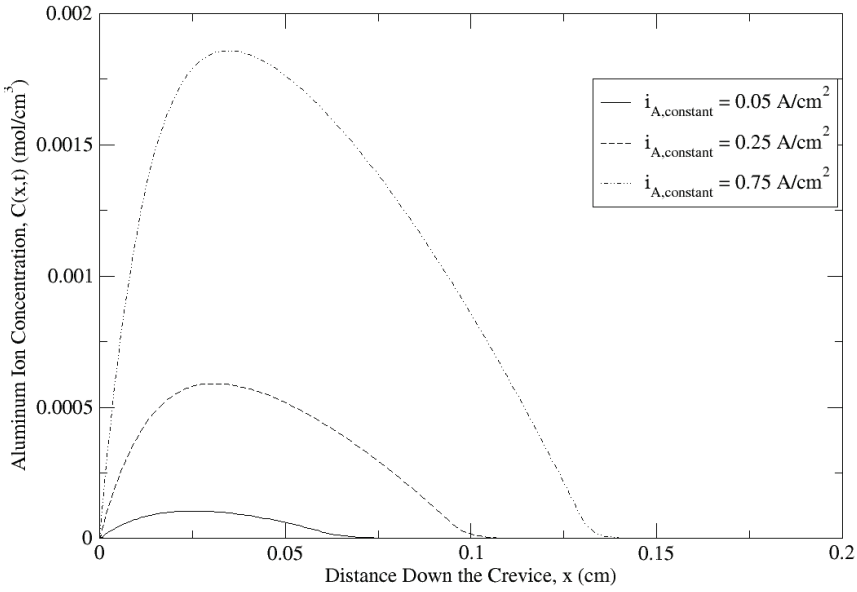

Figure 2.6: The effects of varying current density on the aluminum ion concentration. The concentration of aluminum increases as current density $i_{A,constant}$ increases. Taken from Roland [2].

2.3 Damage Evolution

The final governing equation is for the damage of the aluminum surface. This damage is governed by Faraday's Law, a conservation of mass expression which states the mass lost by a metal is proportional to the charge present,

$$\rho_s h_t = \frac{i_{pit} M}{Fn}. \tag{2.37}$$

Here ρ_s is the density of the solid metal, h_t is the speed at which the pit is growing down into the metal surface, i_{pit} is the current density, F is the Faraday's constant, n is the valence of the metal ion, and M is the molecular weight of the metal. Since $h_t = dh/dt$ we can solve for dh, the change in damage depth, for time step size dt,

$$\frac{dh}{dt} = \frac{i_{pit} M}{Fn\rho_s}. \tag{2.38}$$

As seen in Fig (2.7) the real damage observed in experiments is a smooth profile, and the damage is estimated by $h(x,t)$ with the unidirectional pits of width dx.

2.4 Crevice

As mentioned previously, and shown in Fig (2.3), Roland [2] discusses the crevice region between the steel fastener and aluminum substrate and the damage seen there. In Roland's work the current density value i is unknown over the crevice in the bulk electrolyte. Roland varies the value of i to determine the effects of current density in the crevice on the bulk potential profile. As seen in Fig (2.8) from Roland [2], the

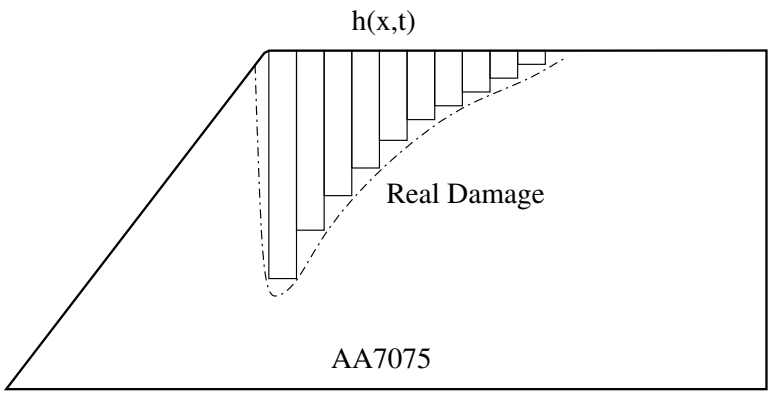

Figure 2.7: Figure of real damage observed versus the estimate of function $h(x,t)$.

bulk potential profile is consistent when the current density at the mouth of the pit is varied from negative, positive, and zero values.

This observation is confirmed by Golovaty's work, [12], solving the Laplace Equation for potential in the entire domain of the bulk and crevice. As seen in Fig (2.9), the potential is almost constant at the mouth of the pit, and thus the current density is also nearly constant at the mouth of the pit. The value used for current density above the crevice mouth is $i_{fixed} =$. This value is provided by Golovaty.

Roland also shows that the bulk current density $i(E)$ can be expressed as a piecewise function

$$i(E) = \begin{cases} -i_c(E) & \text{if} \quad -L_1 \leq x \leq -L_p, \\ i_{fixed} & \text{if} \quad -L_p < x < 0, \\ i_a(E) & \text{if} \quad 0 \leq x \leq L_2. \end{cases} \tag{2.39}$$

Here $-i_c(E)$ is the current density of the steel cathodic surface, $i_a(E)$ is the current density of the aluminum anodic surface, and $i(E) = i_{fixed}$ over the crevice. The

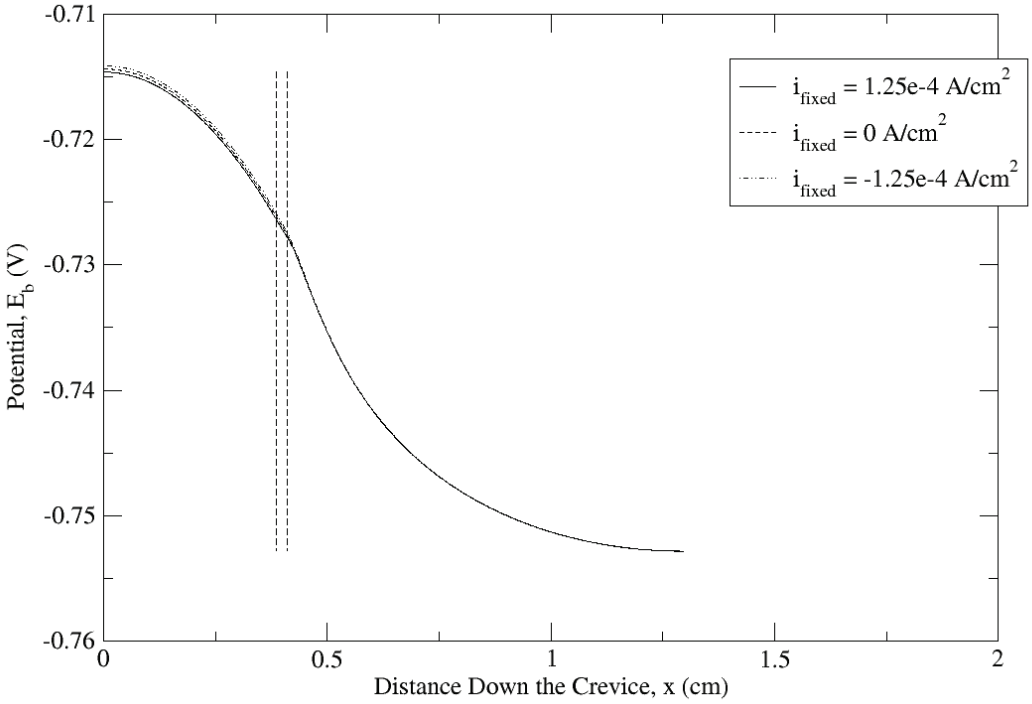

Figure 2.8: The consistent bulk potential profile is demonstrated with varying mouth current density, i_{fixed}. Taken from Roland [2].

spacial value of $x = 0$ represents the edge of the aluminum surface closest to the steel surface, L_2 is the length of the aluminum surface and the right boundary. L_p is the length of the crevice between the metal surfaces, $L_1 - L_p$ is the length of the steel surface, and the negative on both position values represents that the crevice and steel are left of the aluminum. Recall that current density defines the concavity of potential, thus over the crevice the current density profile is positive and is concave up. Hence the couple potential of the galvanic couple exists somewhere near the edge of the steel surface.

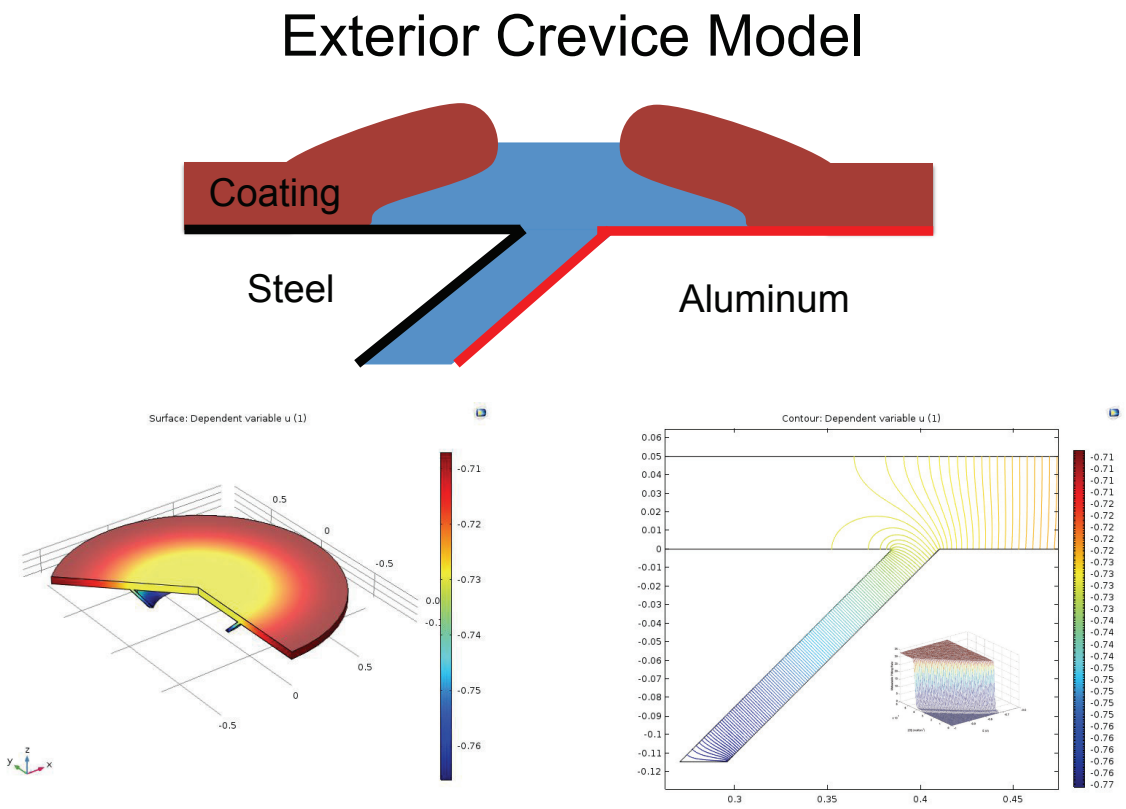

Figure 2.9: Golovaty's results for potential over the crevice, for the specified domain.

2.5 Approach

It is important to note that we have defined i_{pit} as the current density present at the bottom of a pit on the aluminum surface, and that it is present in equations (2.36) - (2.38). Having this specific current density to calculate the damage is unique to our mathematical model. We present three different theories below on how i_{pit} can be calculated. In our model we use the current balance approach for early time. The other two approaches are for oxide formation and repassivation, and are interchangeable in

the model, note that only one is used at a time then compared. The approaches are discussed below.

2.5.1 Current Balance

We start by discussing the Divergence Theorem. The theorem states that the area integral of the divergence of potential through the region of the domain is equal to the outward flux of potential through the surrounding surface. Thus the 2D area integral over the electrolyte domain can be analyzed through boundary line integrals. The Divergence Theorem for potential is expressed as

$$\int\int_R \nabla \cdot \nabla E dA = \int_Y \nabla E \cdot \hat{n} dS. \tag{2.40}$$

Here R is the area where the double integral is defined on the closed bounded 2D domain of the electrolyte, and Y is where the line integral is defined along the smooth piecewise boundaries of the electrolyte. We recall that by the Laplace Equation, the left hand side of equation (2.40) is equal to zero. Thus we have

$$\int_Y \nabla E \cdot \hat{n} dS = 0. \tag{2.41}$$

Similar to Golovaty we use the entire bulk and crevice as our electrolyte domain. To analyze equation (2.41) we recall our discussion of the flux boundary conditions, $\nabla E \cdot \hat{n}$. There is no outward normal flux of potential at the top, left, or right boundaries of the bulk domain. In addition, the assumed inert walls of each pit have no outward normal flux of potential. So in the entire domain of the bulk and crevice, there are outward normal fluxes of potential on the remaining

metal/electrolyte interfaces. Thus, the steel surface in the bulk and crevice, the aluminum surface in the bulk and crevice, and the active bottom pit surface have outward normal fluxes of potential. Hence the line integral, equation (2.41), can be written as the sum over these five surfaces,

$$\int_{Y_1} \nabla E \cdot \hat{n} dS + \int_{Y_2} \nabla E \cdot \hat{n} dS + \int_{Y_3} \nabla E \cdot \hat{n} dS + \int_{Y_4} \nabla E \cdot \hat{n} dS + \int_{Y_5} \nabla E \cdot \hat{n} dS = 0. \quad (2.42)$$

Here Y_1 is the steel surface in the bulk, Y_2 is the surface at the bottom of the pits, Y_3 is the undamaged surface of aluminum in the bulk, Y_4 is the steel surface in the crevice, and Y_5 is the aluminum surface in the crevice. These surfaces are seen in Fig (2.11). By Ohm's Law, eqn (2.12), we have

$$\begin{aligned} \int_{-L_1}^{-L_p} & - \quad i_c(E)dS + \int_0^{L_a} i_{pit}(E)dS + \int_{L_a}^{L_2} i_a(E)dS \\ & + \quad \int_0^{L_{CatCr}} -i_{ccrev}(E)dS + \int_0^{L_{AnCr}} i_{acrev}(E)dS = 0. \end{aligned} \quad (2.43)$$

Here 0 is the edge of the aluminum surface closest to the steel surface, L_2 is the length of the aluminum surface and the right boundary. L_p is the length of the crevice mouth between the metal surfaces, $-L_p + L_1$ is the length of the exposed steel surface, and the negative on both values represents that the crevice and steel are left of the aluminum. The length L_a is the length of active pits on the aluminum surface and is a function of time, $L_a(t)$. The value L_{CatCr} is the length of the steel surface in the crevice, similarly L_{AnCr} is the length of the aluminum surface in the crevice, i_{ccrev} is the cathodic current density in the crevice, i_{acrev} is the anodic current density in the crevice, and dS denotes a line integral over arc length. A diagram of the crevice measurements is shown in Fig (2.11). The values used for i_{acrev} and $-i_{ccrev}$ are from

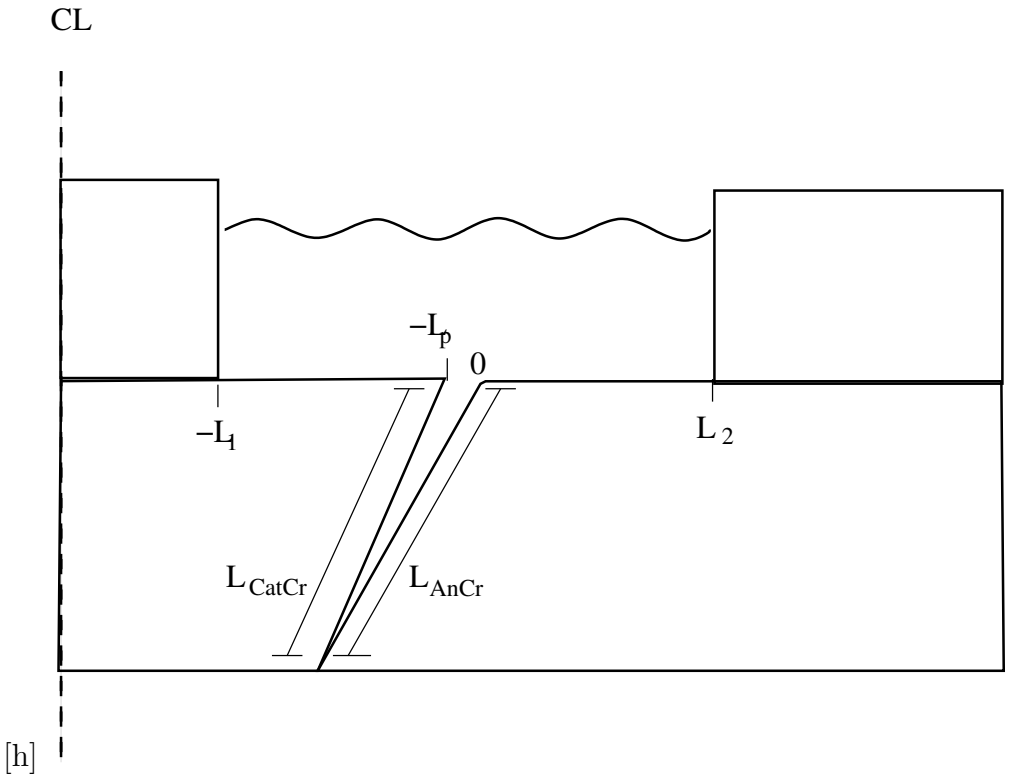

Figure 2.10: The measurements of the crevice that lies between the steel and aluminum surfaces. The 2D area of bulk electrolyte can be seen, as well as the smooth 1D boundary around the electrolyte.

Roland [2]. All important surfaces, measurements and points of the domain can be seen in Fig (2.10) and (2.11).

As done in Brackman [15] we add the equivalent of zero to equation (2.43) and split the equation into two line integrals, one for the bulk electrolyte domain and one for the crevice domain,

$$\int_{-L_1}^{-L_p} -i_c(E)dS \quad + \quad \int_0^{L_a} i_{pit}(E)dS + \int_{L_a}^{L_2} i_a(E)dS + \int_{-L_p}^{0} i_{fixed}dS = 0 \quad (2.44)$$

$$-\int_{-L_p}^{0} i_{fixed}dS \quad + \quad \int_0^{L_{CatCr}} -i_{ccrev}(E)dS + \int_0^{L_{AnCr}} i_{acrev}(E)dS = 0. \quad (2.45)$$

Here i_{fixed} = is the constant current density at the mouth of the pit. We know $i_{fixed} > 0$ from Fig (2.9). The negative integral of i_{fixed} is included in the line integral for the crevice, and the positive integral of i_{fixed} is part of the line integral for the bulk. This is because of the direction of the outward facing normal for the mouth of the pit for each section of the domain. In addition, the crevice balance equation (2.45) shows that the $-\int_{-L_p}^{0} i_{fixed} dS$ and $\int_{0}^{L_{CatCr}} -i_{ccrev}(E) dS$ integrals have the same sign and that the area over the crevice mouth of the crevice subdomain must act as an artificial cathode. Similarly in equation (2.44), the signs of each integral show the area over the mouth of the pit must act as an artificial anode in the bulk subdomain. Thus, the crevice subdomain shows that the crevice anodic current is balancing the cathodic crevice current, plus some of the boldly exposed cathodic surface in the bulk. So the anodic exposed surface is only using part of the exposed cathodic surface current to balance the bulk subdomain. Note that a portion of this cathodic crevice current goes to the corrosion of the aluminum surface in the crevice as discussed in [2].

With the entire domain's current balanced, we focus on the line integral for the bulk domain equation (2.44). We assume i_{pit} and i_{fixed} are constants. Similarly, i_a changes very little over the passive aluminum surface and is estimated as a constant, we say $i_a = i_{Bc}$. Thus we find,

$$\int_{-L_1}^{-L_p} -i_c(E) dS + i_{pit} L_a + i_{Bc} L_u + i_{fixed} L_p = 0. \tag{2.46}$$

We define the length of passive aluminum surface as, $L_u(t) = L_2 - L_a(t)$. Since the value i_{fixed} is small and L_p, the crevice width, is also small, we neglect it. It is

important to note that since the sign of i_{fixed} is known to be positive, we acknowledge that i_{pit} will be overestimated. Thus, the unknown value of i_{pit} is now expressed as

$$i_{pit} = \left(\int_{-L_1}^{-L_p} i_c(E) dS - i_{Bc} L_u \right) / L_a \tag{2.47}$$

This is consistent with the experimental work of [10], who demonstrated the dominant role of the total cathodic current in establishing the anodic current density.

Once again, with the pit current density known, we can calculate the aluminum ions being released and the depth of the damage in each pit. It is important to note, in this approach i_{pit} is the same value in each pit for each time step. In each new time step i_{pit} is calculated, and decreases with time. This occurs because as time passes, more pits initiate, thus $L_a(t)$ increases and i_{pit} decreases. Thus, the pits get deeper by a smaller depth increment each time a new pit initiates. We will determine whether this simulates the profile shape we see in experiments, and accounts for the slowed growth as pits repassivate.

2.5.2 McKinnon

The second approach follows from the work done by McKinnon. McKinnon [1] discusses three stages of pit growth: i) the bulk potential reaches the potential needed for pit initiation, E_P, and pit growth is under ohmic control at a high current density with a pit cover, ii) the pit cover bursts and growth is diffusion controlled under changing current density until the potential at the pit bottom reaches the transition potential, E_T, and iii) growth is ohmic controlled until the potential at the pit bottom reaches the repassivation potential, and extremely low current density. We have

simplified the model to two stages for pits: i) bulk potential is high enough for a pit to initiate and experiences ohmic controlled growth for pit potentials greater than E_T, ii) the pit grows with ohmic controlled growth until the pit potential gets low enough to repassivate the pit. Here the first two growth stages from [1] are modeled as one ohmic controlled growth stage because the diffusion controlled growth of a pit is a short lived stage when the potential is not artificially kept above E_T, the transition potential. Thus, we are assuming the damage done in the diffusion controlled growth stage is insignificant compared to the growth in the ohmic controlled stage. Note that the value of E_T is unknown, and that we estimate the value of E_P using the work by Colwell [3]. As discussed earlier, from the experimental work done in [4], we assume E_T is the potential at which $i_{pit} = 0.005 \frac{amps}{cm^2}$.

Since pits do not form on the steel surface, we only do the following pit calculations along the aluminum surface. Recall that pits are individual entities and grow in one direction, the idealized damage profile is shown in Fig (2.11).

We use the boundary illustrated in the 3D surface, seen in Fig (2.12) from Roland [2] and developed by Colwell [3] as our E_P values. The initiation potential is a function of chloride; as chloride increases initiation potential decreases, as chloride decreases initiation potential increases. The surface from Colwell [3] is 3D, with initiation potential, chloride concentration, and likelihood of pitting each as an axis. There is a steep transition between two flatter areas on the surface, where the top surface represents conditions for pit initiation and the bottom surface represents conditions for a passive aluminum surface.

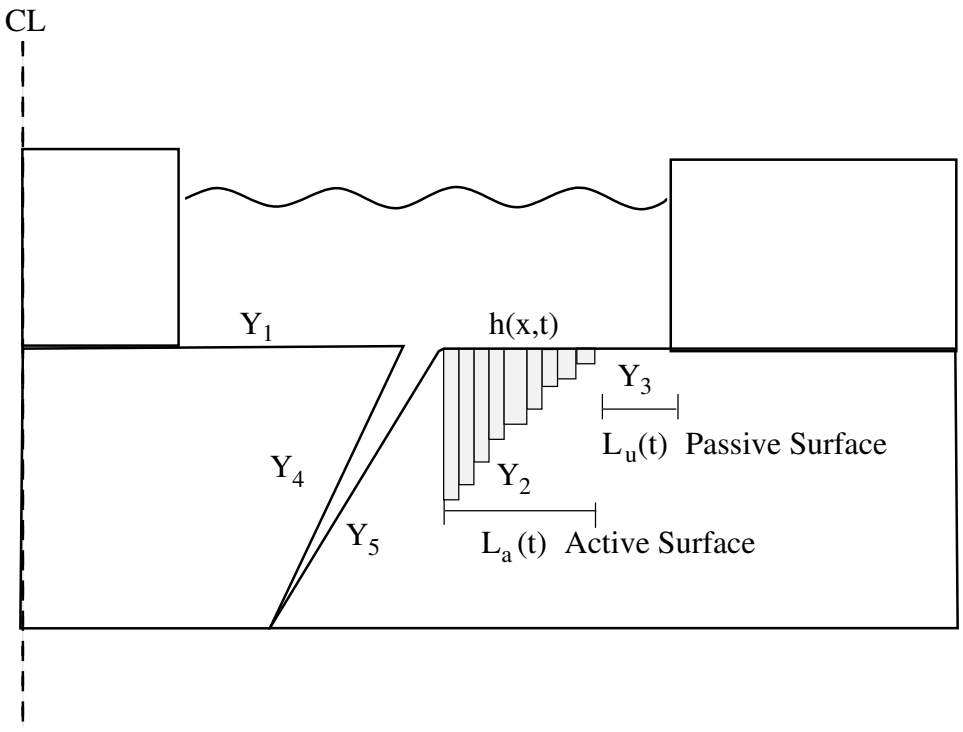

Figure 2.11: An idealization of the damage profile.

We have a linear estimate of the boundary in the potential-chloride concentration plane of the surface, which lies along the steep transition of a pit initiating or not. The boundary has been shifted to give the desired initial length of $L_a(t)$, and to have the correct range of potentials for the system. This boundary is

$$cc = 3.2 \times 10^4 - 0.001142857(E + 1) + 6.5713 \times 10^{-5} \tag{2.48}$$

We represent the chloride concentration from the surface boundary from Colwell [3] as cc. We calculate cc for the calculated bulk potential, E, for each spatial location along the aluminum surface. If the calculated chloride concentration, C, is greater than the corresponding cc then the pit is initiated, otherwise the surface is still passive. This

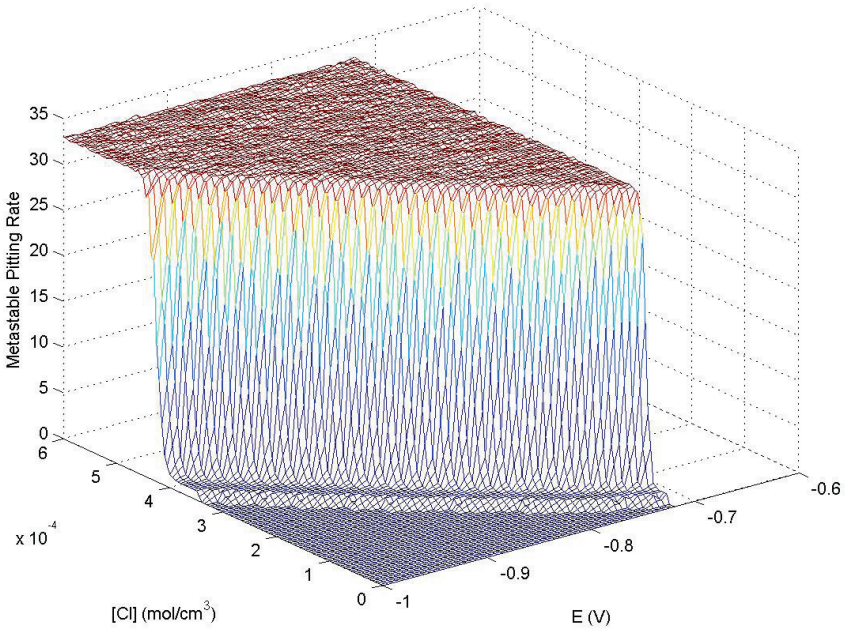

Figure 2.12: The 3D surface of the pit initiation based on chloride concentration and potential developed by Colwell [3].

allows one to determine where there are pits forming on the aluminum surface. The distance marked by $L_a(t)$ is the distance along the aluminum surface, from the crevice mouth, where pits are initiated. Through time $L_a(t)$ increases as more pits start to grow along the aluminum surface.

Next we use equations (2.49) and (2.50) to determine the potential at the bottom of the initiated pits. The equations used are

$$\xi = \frac{-\gamma A_{sat} + \sqrt[2]{\gamma^2 A_{sat}^2 + N a_{blk} C}}{N a_{blk}}, \tag{2.49}$$

$$\Delta E = E - E_{bot} = -\frac{1}{\alpha} ln(\xi). \tag{2.50}$$

A_{sat} is the concentration of aluminum ions the electrolyte can hold in solution. The

value of sodium ions present in the electrolyte is Na_{blk}, and is equal to the initial concentration of chloride, C. The value of γ is prescribed and is a ratio of the electrolyte saturation limit of aluminum ions; it is also the minimum critical chemistry value to have stable growth in the pits. We assume $\gamma = 1$. The value α is the constant representing F/RT. The value ΔE is the potential drop from the bulk to the bottom of the pit at each spatial location. Now that ΔE is obtained we calculate E_{bot} as follows,

$$E_{bot} = E - \Delta E. \tag{2.51}$$

Now that the values of E_{bot} at each spatial location along the aluminum surface are known, we can focus on calculating i_{pit}. With available pit polarization data, such as the data on pure aluminum provided by the Lillard team, the function $i_{pit}(E_{bot})$ can be estimated. The pure aluminum pit polarization curve from Lillard is shown in Fig (2.13). Note that the magnitude of current density in the pit is orders of magnitude larger than that of the corresponding bulk current density at the top of the pit. This agrees with the work done on steel surfaces in [9, 17].

Once the relationship between i_{pit} and E_{bot} is established, through the polarization curve we determine the current density in each pit along the aluminum surface. Furthermore, we calculate the damage depth in each pit once i_{pit} is known using equation (2.38).

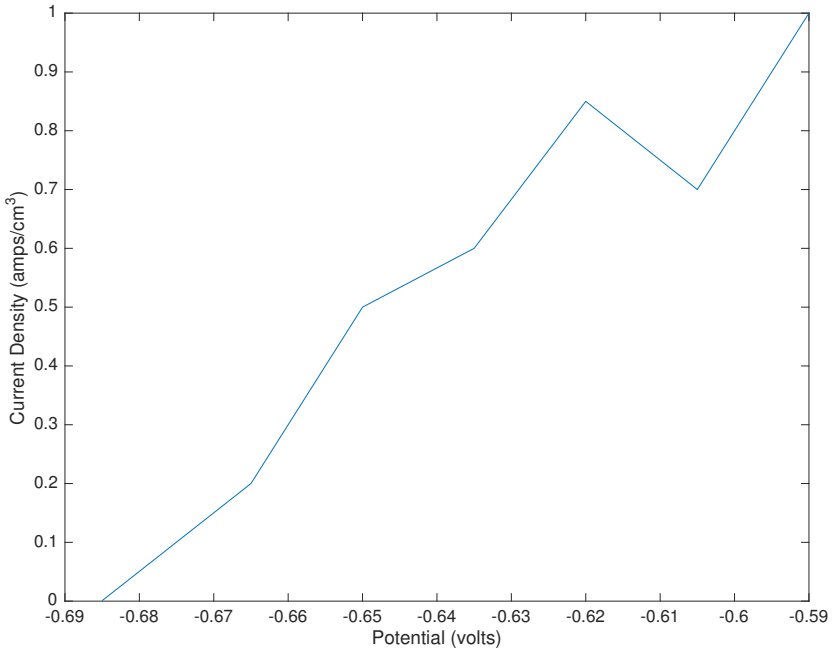

Figure 2.13: For pure aluminum pits, data provided by Lillard, current density as a function of potential.

2.5.3 Single Active Surface

As an alternative to the McKinnon based approach above, this approach is based on [4]. In this approach we assume repassivation starts when the pit current density gets low enough to reach the critical value found from experiment in [4], $i_{pit} = 0.005\frac{amps}{cm^2}$. This current density value represents when the width of the damaged aluminum surface is greater than the depth of the damage, and the pits coalesce. Once, the pits are coalesced the damage in the aluminum acts as a single active surface, and the current density reverts back to corresponding to the bulk polarization. Thus, the current density decreases quickly, the aluminum's dissolution rate decreases, and the

damage growth drastically slows, and the pits repassivate.

2.6 Summary of Governing Equations

The final ODE for the bulk potential is

$$\kappa \left[E_x \cdot (w+h)\right]_x = i(E). \tag{2.52}$$

Since $i(E)$ can be written as $-i_c(E)$ over the steel surface, and as $i_a(E)$ over the aluminum surface, we can express the ODE as the system,

$$\kappa \left[E_x w\right]_x = -i_c(E) \quad \text{for} \quad -L_1 \leq x \leq -L_p, \tag{2.53}$$

$$\kappa \left[E_x w\right]_x = i_{fixed} \quad \text{for} \quad -L_p < x < 0, \tag{2.54}$$

$$\kappa \left[E_x (w+h)\right]_x = i_a(E) \quad \text{for} \quad 0 \leq x \leq L_2. \tag{2.55}$$

By the basic principle of transport phenomena we have the general governing equation for ionic species in a fluid. For aluminum ion concentration we assume diffusion occurs only through the electrolyte, there is a sink term from the formation of aluminum chloride at the mouth of the pit, and there is a surface reaction term for the dissolution of the metal in the pits,

$$A_t = \begin{cases} DA_{xx} + \frac{i_{pit}M}{3F(w+h)} & \text{if} \quad A < 0.003\frac{mol}{cm^3}, \\ DA_{xx} + \frac{i_{pit}M}{3F(w+h)} - KC^3A & \text{if} \quad A \geq 0.003\frac{mol}{cm^3}. \end{cases} \tag{2.56}$$

The algebraic expression from electroneutrality is used to calculate the concentration of chloride,

$$C = 3A + N_{blk}. \tag{2.57}$$

Note that concentrations of other ions like OH^- and H^+ are not tracked in the present model.

The final governing equation defines the damage to the aluminum surface with respect to time,

$$\frac{dh}{dt} = \frac{i_{pit} M}{F n \rho_s}. \tag{2.58}$$

These equations form the system to be solved numerically.

We track the initiation and growth of pits in the first approach, based on the system's current balance and the Divergence Theorem. The expression for current density is

$$i_{pit} = \left(\int_{-L_1}^{-L_p} i_c(E) dS - i_{Bc} L_u \right) / L_a. \tag{2.59}$$

Here i_{pit} is not a function of the potential at the bottom of the pit, E_{bot}. Instead, the current density is a constant for each particular time step, depending on the number of active pits, or length of active surface $L_a(t)$. We use the constant i_{pit} in equations (2.56) and (2.58) to solve the system of equations.

Next we track the formation of oxide and the repassivation of pits with either the second or third approach. Equations (2.49) and (2.50) from [1] are used to calculate the potential drop in each pit, ΔE. Once ΔE is found for each pit, E_{bot} is calculated for each pit. Then we use experimental pit data to determine the current density as a function of potential, $i_{pit}(E_{bot}, t)$. Or, $i_{pit} = i_a(E)$ based on [4] since the pits are assume to coalesce and act as a single active surface where local current density has reverted back to bulk current density values. The calculated pit current

density, based on the chosen approach, is then used to solve equations (2.56) and (2.58).

2.7 Table of Parameters and Variables

Table 2.1 summarizes the symbols and units used here, while Table 2.2 provides baseline values of the parameters.

Table 2.1: Variables and Units.

Name	**Variable**	**Units**
Concentration of i-th species	C_i	$\frac{mol}{cm^3}$
Flux of species	J	$\frac{mol}{cm^2}$
Mass Diffusion coefficient of i-th species	D_i	$\frac{cm^2}{s}$
Valance of i-th species	n	$+/-$ electrons
Velocity vector	$\bar{u}$	$\frac{cm}{s}$
Bulk Potential	E	$volts$
Bottom Pit Potential	E_{bot}	$volts$
Potential Drop	ΔE	$volts$
Outward Normal vector	$\hat{n}$	none
Length of passive Al surface	$L_u(t)$	cm

Name	**Variable**	**Units**
Mass transfer coefficient	$\hat{K}$	$\frac{cm}{s}$
Source term	S^+	$\frac{mol}{cm^3 s}$
Sink term	S^-	$\frac{mol}{cm^3 s}$
Damage profile	$h(x,t)$	cm
Chloride Concentration	$C(x,t)$	$\frac{mol}{cm^3}$
Aluminum Ion Concentration	$A(x,t)$	$\frac{mol}{cm^3}$
Colwell Surface Chloride	cc	$\frac{mol}{cm^3}$
Bulk Current Density	$i(E)$	$\frac{amp}{cm^2}$
Cathodic Current Density	$-i_c(E)$	$\frac{amp}{cm^2}$
Anodic Current Density	$i_a(E)$	$\frac{amp}{cm^2}$
Pit Current Density	i_{pit}	$\frac{amp}{cm^2}$

Note that the value of A_{sat} is an estimated value based on the solubility limit from Fig (2.5).

Table 2.2: Parameters and Values.

Name	**Parameter**	**Value**	**Units**
Faraday's Constant	F	96485	$\frac{Amp \cdot s}{mol}$
Universal Gas Constant	R	8.314	$\frac{J}{mol \cdot K}$
Temperature	T	295	K
Conductivity of electrolyte	κ	0.956938	$\frac{Amp}{Volt \cdot cm}$
Electrolyte thickness	$w(x)$	1	cm
Length of Al surface	L_2	0.3	cm
Length of crevice opening	L_p	0.01	cm
Left boundary distance	L_1	0.3	cm
Initial length of active Al surface	$L_a(0)$	0.0003	cm
Molecular weight of Al	M	26.98	$\frac{g}{mol}$
Density of AA7075	ρ_s	2.81	$\frac{g}{cm^3}$
Solution saturation of AA7075	A_{sat}	0.005	$\frac{mol}{cm^3}$
Bulk Sodium Concentration	Na_{blk}	0.0001	$\frac{mol}{cm^3}$
Current Density from OPC of AA7075	i_{Bc}	10^{-7}	$\frac{mol}{cm^3}$

CHAPTER III

NUMERICS AND SOLUTION PROCEDURE

3.1 Numerics

Equations (2.52), (2.56), (2.57), and (2.58) are the main equations used in modeling the damage to the aluminum surface over time. In addition, we utilize; the 3D surface from Colwell [3] to determine pit initiation, experimental data from the Lillard team's pitting experiment to determine the pit current density as a function of pit potential, equations (2.49) and (2.50) from McKinnon [1] to determine the potential at the bottom of each pit, and the critical current density value and repassivation theory from [4]. We include a current balance formulation, a function based on pit experiments, and a function based on bulk experiments, for calculating i_{pit}, the current density present in the pits. Fortran is the platform used to develop and run simulations of the model. Matlab is used for graphing the data files produced. The model uses the finite differences method and the Crank-Nicolson method with uniform spacial dx, and uniform time dt, stepping. A pseudo-time loop is used to reach a steady state profile of the potential in the bulk electrolyte using uniform time stepping with $d\tau$. A memory saving format is used for the arrays tracking potential, chloride, and aluminum concentration, depth of electrolyte, and damage.

The equation used for current density in the bulk electrolyte is listed below,

$$i(E) = \begin{cases} i_a = 1.949 \times 10^{-5} + \frac{(E+.75049)(4.122\times10^{-5}-1.949\times10-5)}{(-.74891+.75049)} & \text{if} \quad x \geq 0\text{cm}, \\ -i_c = -2.46 \times 10^{-5} - \frac{(E+.74335)(2.568\times10^{-5}+2.46\times10^{-5})}{(-.75514+.74335)} & \text{if} \quad x < -L_p. \end{cases} \tag{3.1}$$

This equation is developed to reflect the data set from the Lillard team. In Fig (3.1), $i(E)$ is compared to experimental data. Here $i(E)$ is the current density present on the metal surface in the bulk electrolyte, and is dependent on the potential in the bulk, E, at the metal surface. This expression for bulk current density is used to find the steady state potential profile in the bulk. The following section outlines the solution procedure to solving the governing system of equations and the damage profile of the aluminum surface over time. The damage profiles we develop will also be compared to experimental damage profiles and to computed profiles based on previous investigations, where $i(E)$ is the current density used to predict damage.

3.2 Solution Procedures

The numerical simulation algorithm consists of 3 main sections, described below.

The pseudo-time loop: The steady state potential ODE, equation (2.52), is artificially converted to a parabolic PDE by introducing the pseudotime τ dependent term, E_τ.

$$E_\tau = (E_x \kappa(w+h))_x - i(E) \tag{3.2}$$

The equation is run to its steady state value using uniform time $d\tau$. The steady state profile is used as the fixed potential in the remainder of the problem. Note

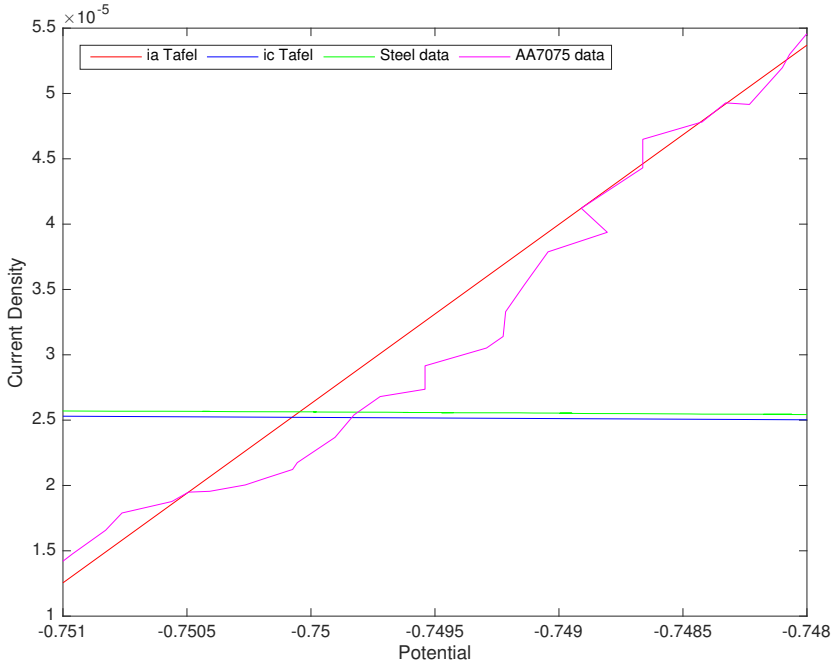

Figure 3.1: The Tafel curves developed compared to the data set from Lillard's team.

that experimentations indicate that the potential does not change appreciably. So, potential, E is initialized with a linear estimate of the bulk potential profile. While the L2-norm is greater than the tolerance level, calculate the potential, E, at each position x. Solve equation (3.2) using Crank-Nicolson, and terms $h(x,t)$ and $i(E(x),t)$ are lagged by one time step. Thus, in each time step, values at time step $p+1$ are being calculated based on known values from the previously calculated time step p.

The pit growth scheme: For early time, when $A < 0.003\frac{mol}{cm^3}$, the aluminum concentration is too low for the bulk reaction to occur; hence equation (2.56) is used to calculate the aluminum concentration. Here the current balance approach developed in Chapter 2 is utilized. Thus, the value of i_{pit} for each time step is a constant

based on a current balance. Total current can be calculated from the product of current density and area. Since we assume the system is one unit in depth, the area is equal to the length of the metal surface. In the system the total current over the steel surface must equal the total current over the aluminum surface. For steel, the current density and length are known. As for the aluminum surface we consider the surface area in two parts, active or passive. The length of the passive area is calculated as $L_u(t) = L_2 - L_a(t)$, and the current density over that length is assumed to be uniform. This is because the potential drop over this length is small, so we use the current density at the far right of the system as the constant value. For aluminum the active area length is known, and as described below the only unknown in the relationship is i_{pit}, the current density present in the active area. This current balance yields the expression,

$$i_{pit} = \frac{I_c - L_u(t) i_{Bc}}{L_a(t)}, \tag{3.3}$$

where I_c is the total cathodic current at the steel surface, $L_u(t)$ is the length of the passive area of aluminum, i_{Bc} is the current density of AA7075 far from the couple, its open circuit potential, and $L_a(t)$ is the length of the active area of aluminum. When the length of the active area is small, especially in the beginning when the first pit initiates, i_{pit} is large. With this high current density, the initiated pits have a greater damage. As more pits are initiated the length of active surface is larger and i_{pit} becomes smaller. This causes all initiated pits to experience a slower damage growth rate as time passes.

In order, the boundary cc is calculated, $L_a(t)$ and the index for the active area are incremented, and $L_u(t)$ is updated. Then the total cathodic current is calculated. This allows the value of i_{pit} to be calculated with equation (2.59) for the corresponding time step. The concentration of aluminum ions, A, is then calculated with Crank-Nicolson without the sink term, equation (2.56). The concentration of chloride, C, at each position x can be calculated for algebraically given time step n with equation (2.57). Finally, the damage, h, is calculated using equation (2.58).

The repassivation scheme: When the aluminum concentration reaches the threshold of $0.003\frac{mol}{cm^3}$, or the pit current density decreases to the critical value of $0.005\frac{amps}{cm^2}$, the bulk reaction begins to occur, so equation (2.56) is used to compute the aluminum concentration. There are two possible ways to calculate pit current density in this scheme:

i) The current balance model is replaced by the McKinnon model to compute $i_{pit}(E)$, based on Fig(2.13) and the results from McKinnon [1].

In order for each time step, the same procedure for cc, $L_a(t)$, and $L_u(t)$ as in the pit growth scheme, is done. Then the change in potential is calculated, ΔE, between the top and bottom of the pit at each position x, using McKinnon's equations (2.49) and (2.50). Then calculate the potential at the bottom of each pit, $E_{bot} = E - \Delta E$, for every position x, using E and ΔE, where E is the potential at the top of the pit. The concentration of aluminum ions, A, is then calculated with Crank-Nicolson. The concentration of chloride, C, at each position x can be calculated with equation (2.57) with electroneutrality. Finally, the damage, h, is

calculated dependent on $i_{pit}(E_{bot})$ with equation (2.58).

ii) The current balance model is replaced with the single active surface approach from [4]. Hence, $i_{pit} = i_a(E)$.

For each time step, the same procedure for cc, $L_a(t)$, and $L_u(t)$ as in the pit growth scheme, is done. Then $i_a(E)$ from the bulk polarization curve is used to calculate the concentration of aluminum ions, A, with Crank-Nicolson. Chloride, C, is calculated with electroneutrality. Finally, the damage, h, is calculated with $i_a(E)$.

A diagram of a sample of the algorithm using the McKinnon approach is shown below in Fig (3.2). Note that the repassivation scheme i) utilizes a function for the current density in the pit that is dependent on the potential at the bottom of the pit. This function comes from relevant experimental data showing the relation of pit potential and current density. This data is unavailable for AA7075 and stainless steel, so we model the function based on [1] and the pure aluminum pit data trends in Fig (2.13) to postulate a profile for AA7075.

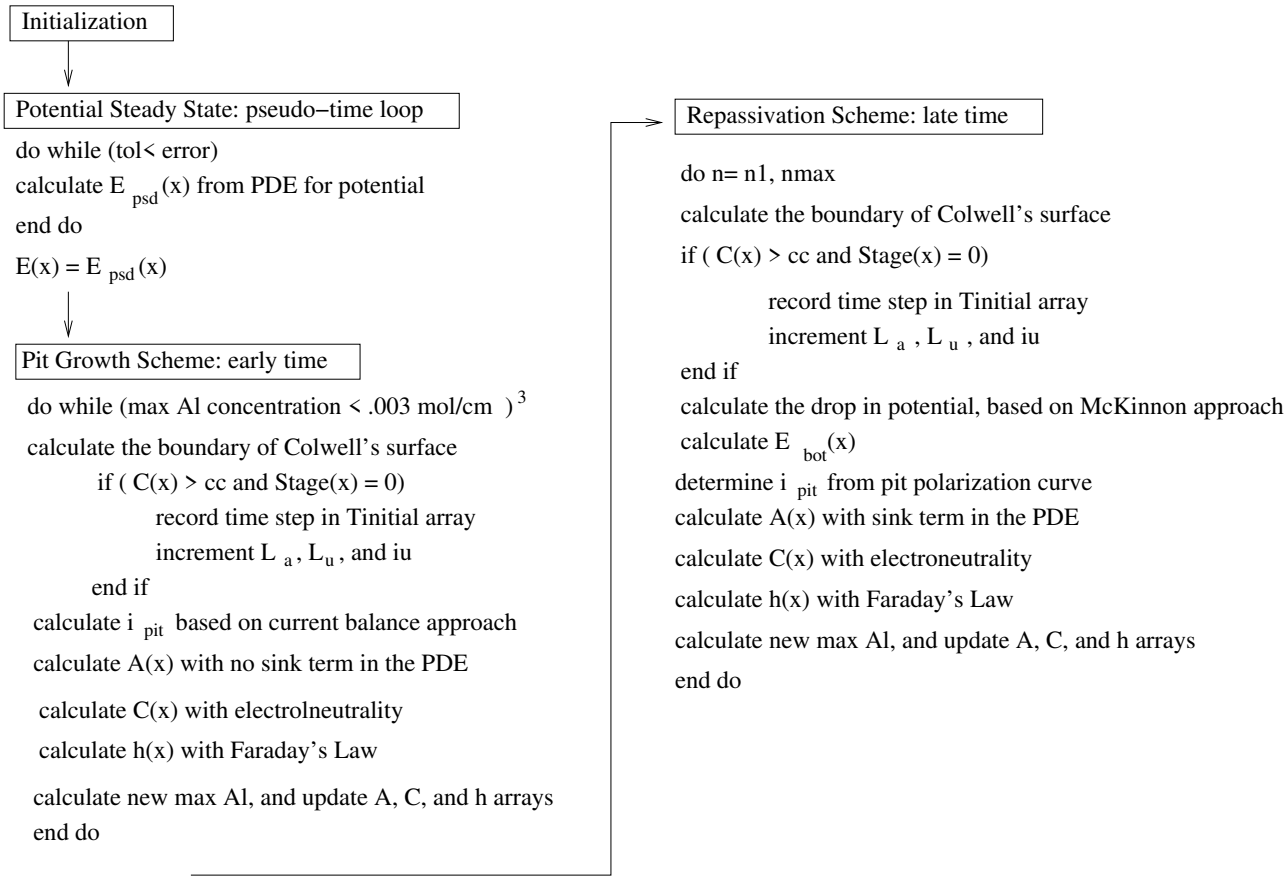

Figure 3.2: A flow chart and pseudocode of model algorithm developed.

CHAPTER IV

CONCLUSION

4.1 Conclusion

The work presented in this paper includes the derivation of a 1D mathematical model predicting the damage profile of galvanically induced pitting corrosion on AA7075 when coupled with a stainless steel fastener assembly. This model describes the physical situation where the coating over an aluminum surface with stainless steel bolts is damaged and the dissimilar metal couple is exposed. The electrolyte in contact with the metal surface is saltwater with a concentration of $0.1M$ of NaCl. The other ionic species present in the system are not tracked.

Under well-mixed assumptions the Nernst-Planck Equation is reduced to the Laplace Equation for the potential in the bulk electrolyte. No flux boundary conditions are applied to the passive surfaces of the domain, and Ohm's Law is used as the boundary condition on the bottom pit surface, where the metal/electrolyte interface is reactive. The Laplace Equation for the potential in the electrolyte is reduced to a one-dimensional equation, through integration as in the work of Stenta [5]. The final ODE for potential is equation (2.52),

$$\kappa \left[E_x \cdot (w + h)\right]_x = i(E).$$

The concentration of aluminum ions is described by the PDE, equation (2.56),

$$A_t = \begin{cases} DA_{xx} + \frac{i_{pit}M}{3F(w+h)} & \text{if} \quad A < 0.003\frac{mol}{cm^3} \\ DA_{xx} + \frac{i_{pit}M}{3F(w+h)} - KC^3A & \text{if} \quad A \geq 0.003\frac{mol}{cm^3} \end{cases}$$

The concentration of chloride is then described by electroneutrality, equation (2.57),

$$C = 3A + N_{blk} \tag{4.1}$$

Faraday's Law is used to describe the corrosion rate of the aluminum surface, equation (2.58),

$$\frac{dh}{dt} = \frac{i_{pit}M}{Fn\rho_s}.$$

This system of equations can predict the damage profile of the AA7075 surface through time. Fortran is used as the computing platform, and Matlab is used to plot outputs, giving a full description of the predicted damage profile.

Summary of Major Assumptions:

• Well-mixed electrolyte: $w >> h$ thus the electrolyte is considered thick and the assumption is used to simplify the Nernst-Planck equation to the Laplace Equation;

• No flux through exterior boundaries or inert walls on pits: no change in the potential through those surfaces;

• No mass transfer of ionic species: the aluminum and chloride ions are not entering or leaving the system at the exterior boundaries;

• Thin film electrolyte: electrolyte length, L, is much larger than the electrolyte depth, w, implying $\frac{w}{L} << 1$;

• Inert pit walls: each pit is its own entity and behaves like a pencil electrode and corrodes in one direction;

• Potential is independent of time and nearly constant at each position x.

4.2 Future Work

In the continuation of this research, the model proposed should be solved, tested, and compared to available experimental data, from [10, 11], for the damage of aluminum alloys and stainless steel couples.

The model proposed in this honor's project should be run to simulate damage in the AA7075 surface over 3 days. With dt equal to one second, the model should be run for about 260,000 time steps.

Three different damage profiles should be investigated. Equations (2.56) and (2.58) depend on current density, thus the damage profile can be varied by changing the input current density. Three different current density trials should be run: i) where current density is based on the bulk polarization curve only, $i_a(E)$, ii) with the current density, i_{pit}, as proposed in Section 2.5.1 and 2.5.2, iii) use current density i_{pit} for the pit growth scheme of the model, then use $i_a(E)$ for the repassivation scheme of the model as described in Section 2.5.3. The results of these three trials should be compared to experimental data of damage provided by Lillard and his team.

The expected outcome for the first trial would be a drastic underestimation of the depth of the pits compared to experiments. For the second trial we would expect the damage depth to be a slight overestimation of pit depth. Finally, for the

third trial, we would expect the damage depth to be less than the second trial and possibly the closest to the experimental damage observed.

Further work could include solving the Laplace Equation for a 2D system, eliminating the thin film electrolyte assumption. Systems where potential changes vertically through the bulk electrolyte would benefit from this higher dimension approach.

It is also important to expand the number of ionic species. Some systems cannot be assumed to have well-mixed electrolyte, and all species concentrations must be tracked throughout the domain. This introduces the need for the Nernst-Planck Equation to be solved for each species.

For atmospheric corrosion, one needs to solve the original system of electroneutrality and the PDE's for aluminum and chloride with the electromigration terms present. This should be done following the work done by Stenta [6]. The potential profile would not be assumed to be nearly constant and would change with time.

BIBLIOGRAPHY

[1] J.M. McKinnon. Modeling unidirection corrosion damage evolution in a pencil-electrode pit. Master's thesis, University of Akron, 2016. unpublished thesis.

[2] Z.R. Roland. Galvanically induced/accelerated crevice corrosion. Master's thesis, University of Akron, 2016.

[3] A.M. Colwell. Development of a stochastic metastable pit initiation model with transition to a stable pit state. Master's thesis, University of Akron, 2016.

[4] Z. Haque, B.A. Clark, and R.S. Lillard. Experimental considerations for modeling galvanic corrosion in aluminum and its alloys. submitted to Corrosion, 2018.

[5] A.J. Stenta. One dimensional approach to modeling damage evolution in galvanic corrosion. Master's thesis, University of Akron, 2013.

[6] G.S. Frankel and Zhicao Feng. Galvanic test panels for accelerated corrsion testing of coated al alloys: Part 2 - measurement of galvanic interaction. *Corrosion*, 70:95–106, January 2014.

[7] N.J. Laycock and R.C. Newman. Localised dissolution kinetics, salt films and pitting potentials. *Corrosion Science*, 39:1771–1790, 1997.

[8] J.R. Galvele. Transport processes and mechanism of pitting of metals. *J. Electrochem. Soc.: Electrochemical Science and Technology*, 123:464–474, April 1976.

[9] G.S. Frankel, L. Stockert, F. Hunkeler, and H. Boehni. Metastable pitting of stainless steel. *Corrosion*, 43:429–436, July 1987.

[10] G.S. Frankel, C.A. Matzdorf, W.C. Nickerson, B.C. Rincon Troconis, Longfei Li, and R.G. Buchheit. Galvanic test panels for accelerated corrsion testing of coated al alloys: Part 1 - concept. *Corrosion*, 69:1240–1246, December 2013.

[11] G.S. Frankel and Zhicao Feng. Galvanic test panels for accelerated corrsion testing of coated al alloys: Part 2 - measurement of galvanic interaction. *Corrosion*, 70:95–106, January 2014.

[12] D. Golovaty. Personal communication.

[13] M.K. Cavanaugh, N. Birbilis, and R. Buchheit. A quantitative study on the effects of environment and microstructure on pit initiation. *ECS Transactions*, 16:1–11, 2009.

[14] A.S. Elola, T.F. Otero, and A. Porro. Evolution of pitting of aluminum exposed to the atmosphere. *Corrosion*, 48:854–863, 1992.

[15] M.D. Brackman. Modeling and simulation of damaged evolution in crevice corrosion. Master's thesis, University of Akron, 2012.

[16] D. Mizuno and R.G. Kelly. Galvanically induced intergranular corrosion of aa5083-h131 under atmosphere exposure conditions: Part 1 - experimental characterization. *Corrosion*, 69:580–592, June 2013.

[17] D. Mizuno and R.G. Kelly. Galvanically induced intergranular corrosion of aa5083-h131 under atmosphere exposure conditions: Part 2 - modeling of the damage distribution. *Corrosion*, 69:681–692, July 2013.